



Letter

Low-temperature processing of a solution-deposited CuInSse thin-film solar cell

William W. Hou^a, Brion Bob^b, Sheng-han Li^a, Yang Yang^{a,*}^a Department of Materials Science and Engineering, University of California-Los Angeles, Los Angeles, CA 90095, USA^b Department of Physics, Harvard University, 17 Oxford Street, Cambridge, MA 02138, USA

ARTICLE INFO

Article history:

Received 14 May 2009

Received in revised form 16 June 2009

Accepted 17 June 2009

Available online 26 June 2009

Keywords:

Non-vacuum

Spin-coating

Solar cell

Photovoltaics

Hydrazine

CuInSse

ABSTRACT

A low-temperature (~ 350 °C) solution-processed CuInSse photovoltaic cell is reported. The CuInSse film was solution-deposited via spin-coating from a precursor solution consisting of metal chalcogenides (Cu_2S and In_2Se_3) dissolved in hydrazine (N_2H_4). X-ray diffraction data indicated a full conversion from the hydrazine precursor to $\text{CuInS}_x\text{Se}_{2-x}$ structure at 350 °C with an average crystallite size of approximately 45 nm. Bandgap tuning of the $\text{CuInS}_x\text{Se}_{2-x}$ was achieved by varying the excess amount of sulfur in the precursor solution. Based on the (220) reflection of the XRD pattern, the bandgap of $\text{CuInS}_x\text{Se}_{2-x}$ ranged from 1.00 to 1.14 eV. Standard testing conditions at 1-sun intensity resulted in a power conversion efficiency of 7.43%.

Published by Elsevier B.V.

1. Introduction

The ability to fabricate light-weight and flexible photovoltaic cells with scalable processing has initiated numerous research activities in the solar community. Among the various materials, chalcopyrites, such as CuInSe_2 (CIS), CuIn(S,Se)_2 (CISS), and Cu(In,Ga)Se_2 (CIGS) have attracted considerable attention. These materials have an absorption coefficient on the order of 10^5 cm^{-1} , which translates to 90% absorption with 200-nm thickness [1]. This property renders the chalcopyrites advantageous for weight considerations. However, the standard thickness of the chalcopyrite layer in a solar cell is presently 1.5–2 μm [2], and a thinner absorber layer thickness is generally associated with an increase in shunt conductance. The shunting is a result of surface roughness on the same order as film thickness [3–4]. In addition to decreasing the chalcopyrite thickness, replacing soda-lime glass with polyimide substrates would provide further advantages in reducing the weight of the device and also the possibility of being flexible. Given that the glass-transition temperature of polyimide is approximately 400 °C, adopting the conventional deposition methods for CIS, such as coevaporation or electrodeposition, has been shown to be challenging [5].

Recently, a solution processing of CIGS method has been demonstrated using hydrazine as a solvent [6]. The chalcopyrite layer, processed at 470 °C, has been shown to have a photovoltaic efficiency of 10.2%. In the present work, we explore two facets of this hydrazine-processing method. First, the low-temperature regime of the transformation process is studied. After dissolving the metal chalcogenides in hydrazine, the solutions can be applied directly to a substrate to form smooth and dense films. Upon heating at 350 °C, the precursor film is converted to the chalcopyrite structure, and can then be subjected to further treatment. Second, the formation of CISS by incorporating sulfur (S) in the precursor solution is investigated. This method not only provides a low-temperature processing of chalcopyrite materials, but also demonstrates a simplified route of forming CISS by avoiding an additional chalcogenization step that is necessary in the traditional methods.

2. Experimental details

2.1. Solution preparation

Prior to forming the precursor solution, 1 mmol of copper sulfide (Cu_2S) and 2 mmol of sulfur (S) were combined with 4 mL of hydrazine. In a separate vessel, 1 mmol of indium selenide (In_2Se_3) and excess S or selenium (Se) were combined with 4 mL of hydrazine. A more detailed description of the precursor synthesis has been reported previously [7]. After several days of continuous stirring at room temperature, the suspensions of Cu_2S and In_2Se_3 formed clear

* Corresponding author. University of California-Los Angeles, Department of Materials Science and Engineering, Los Angeles, CA 90095, United States. Tel.: +1 310 825 4052; fax: +1 310 825 3665.

E-mail address: yangy@ucla.edu (Y. Yang).

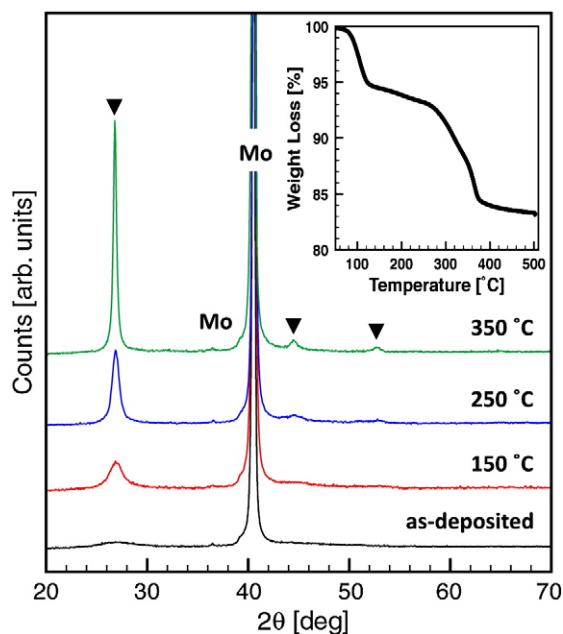


Fig. 1. X-ray diffraction of the precursor films deposited on the Mo substrate, which were subsequently thermally annealed at 150, 250, and 350 °C. Reflections of CuInS₂Se are marked with (▼). Inset: thermogravimetric analysis of the precursor material measured under a heating rate of 2 °C/min.

yellow and colorless solutions, respectively. It was noted that the dissolution of In₂Se₃ in the presence of excess chalcogen is accompanied by a noticeable increase in viscosity. Both solutions were filtered to remove any insoluble species, and were subsequently mixed to form the precursor solution. Figures that contain images of all three solutions can be found in a report by Hou et al. [8]. The amount excess chalcogen (S or Se) in the In₂Se₃ solution is varied depending on the desired chalcogen content in the resulting material.

2.2. Device fabrication

The fabrication of the photovoltaic cell began with the deposition of molybdenum (Mo, 1000 nm) onto a Corning 2947 glass slide by argon dc sputtering. The processing pressure was varied during deposition to achieve a bi-layer microstructure, as has been reported in the literature [9]. The CuInS_xSe_{2-x} layer was deposited by spin-coating the precursor solution onto the Mo layer, followed by thermal annealing at 350 °C for 60 min. The deposition of the CuInS_ySe_{2-x} layer was repeated several times, one layer on top of another, in order to achieve a film thickness of approximately 600 nm. The Cu:In concentrations were kept constant for all three depositions. Both deposition and annealing were carried out in a nitrogen-filled glove box. Next, the cadmium sulfide (CdS) layer was deposited by chemical bath deposition. Finally, 30 nm of intrinsic zinc oxide (ZnO) and 120 nm of indium tin oxide (ITO) were deposited by argon rf sputtering, and served as the top transparent electrode. The total area of the cell was 0.18 cm², as defined by the shadow mask used during sputtering.

2.3. Characterization

The photovoltaic performance was characterized in air without any encapsulation under an AM1.5G filter at 100 mW/cm² using a Newport Oriel 92192 Solar Simulator. The intensity of the light source was calibrated with an NREL-calibrated reference diode [10]. All X-ray diffraction samples (XRD) were prepared using the same deposition profile as that described for the photovoltaic cell fabrication. The XRD patterns were collected on a PANalytical X'Pert Pro X-ray Powder

Diffractometer using Cu-Kα radiation ($\lambda = 1.54050 \text{ \AA}$). The scanning electron microscope (SEM) images were taken on a Joel JSM-6700F that is equipped with an energy dispersive X-ray (EDX) analyzer based on a lithium drifted silicon detector (SiLi-204R2). Both the SEM images and EDX spectra were taken with an accelerating voltage of 10 kV.

3. Results and discussion

XRD patterns of the as-cast precursor film as well as films annealed at 150, 250, and 350 °C are shown in Fig. 1. The as-cast precursor film was prepared by placing the spin-coated precursor film in an antechamber overnight under vacuum. The XRD pattern of the as-cast film appeared to be amorphous, which is in good agreement with that reported previously [7]. As the temperature increased to 150 °C, the three reflections ((112), (220), and (312)) of the CuInS₂Se structure became apparent. The presence of these reflections suggested that a certain amount of CuInS₂Se crystallite is present even at 150 °C. At 250 °C, the patterns can be clearly indexed to be CuInS₂Se structure (JCPDS 36-1311). At 350 °C, the pattern essentially follows that of the pattern obtained at 250 °C, except with a decrease of full-width at half-maximum (FWHM), which indicates an increase in grain size. Based on FWHM of the (112) reflection, the estimated grain size is increased from 21.5 nm for the film annealed at 250 °C to 45.5 nm for the film annealed at 350 °C. Annealing at temperatures above 350 °C have resulted in ~100 nm grain size due to coarsening. However, given the formation of CISS crystallites at relatively low temperature, it is not possible to reach ~ μm grain size by coarsening alone. Based on the observations in the XRD patterns at various temperatures, it is suggested that the reaction pathway of this hydrazine-derived CISS is different from that of reacting metal chalcogenides at elevated temperature. Perhaps this is the reason why CISS reflections are present at temperatures as low as 150 °C. This lower annealing temperature can be beneficial to achieve uniform distribution of Cu and In over a large area, which is critical to improving the overall efficiency of a solar module.

In an attempt to increase the bandgap by substituting S in the Se sites of the CISS structure, the amount of excess S in the precursor solution was varied to achieve S/[S+Se] mole ratios of 0.4, 0.5, and 0.6. Fig. 2 shows the XRD of CISS films spin-coated using precursor solutions with different sulfur content, which were subsequently thermally annealed at 350 °C. The position of the (220) reflection shifts to higher 2 θ value as the sulfur content increases. This is

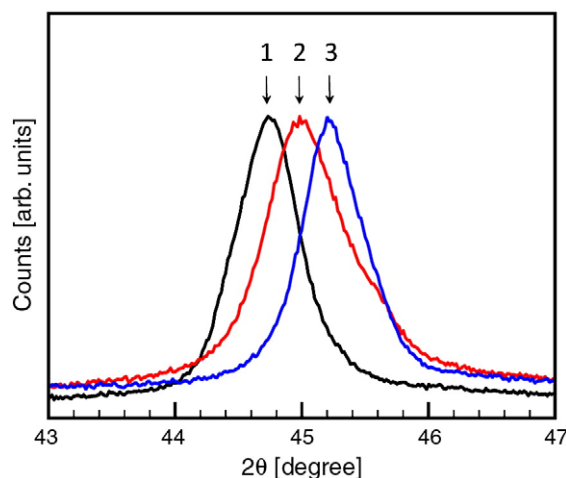


Fig. 2. The (220)/(204) reflection of CuInS_xSe_{2-x} (annealed at 350 °C) using powder X-ray diffraction. The peak intensities are normalized to assist in comparison of peak positions. Different sulfur content for samples 1, 2, and 3 were prepared by varying the S/Se ratio in the precursor solution using mole fractions of sulfur of 0.4, 0.5, and 0.6, respectively.

Table 1

Comparison of the sulfur mole fraction in the precursor solution prior to annealing and after annealing at 350 °C.

Sample	S/[S + Se] initial	S/[S + Se] annealed	E_g (eV)
1	0.4	0.04	1.06
2	0.5	0.13	1.10
3	0.6	0.22	1.14

The post-annealed mole fraction and the bandgap values are calculated based on the (220)/(204) of the XRD patterns.

indicative of decreasing d-spacing, as would be expected with increasing sulfur substitution in the crystal lattice. The amount of sulfur in the thermally annealed films was derived by choosing the (220) reflection to avoid any contributions from the c-direction in the lattice. The calculated values of S/[S + Se] were 0.04, 0.13, and 0.22 based on the original ratios of 0.4, 0.5, and 0.6, respectively, in the precursor solutions. A summary of the S/[S + Se] values can be found in Table 1. Assuming a linear relationship between the bandgap values for that of CuInSe_2 (1.02 eV [11]) and CuInS_2 (1.53 eV [12]), the bandgaps of the resulting films are calculated to be 1.06, 1.10, and 1.14 eV, respectively, for the initial S/[S + Se] ratios of 0.4, 0.5, and 0.6. The presence of impurity phases is likely to occur as sulfur content increases. This can be observed for Sample 2, as indicated by the presence of a shoulder in the peak.

Based on the S/[S + Se] ratio between the initial amount to that after thermal annealing at 350 °C, it can be concluded that only a limited amount of sulfur is incorporated. To understand the origin of the loss of S, the film composition was measured at various annealing temperatures using EDX, as shown in Fig. 3. The initial S/[S + Se] ratio in precursor solution was chosen to be 0.5, which corresponds to the mole fraction of sulfur content in CISS. A significant amount of S was lost in the precursor film at temperatures as low as 50 °C. Similar losses were also observed in precursor films that were not subjected to any thermal treatment. This suggested that sulfur loss might occur during the precursor preparation when it came in contact with hydrazine. It is likely that the sulfur is lost as hydrogen sulfide, which is a common byproduct during the reaction of hydrazine and sulfur [13]. For temperatures above 50 °C, there is continual loss of S, and the amount lost seemed to not increase at temperatures beyond 150 °C. The EDX result on the S/Se ratio of the sample annealed at 350 °C also agrees with that calculated from the XRD patterns. This result suggested that there is a limited solubility of elemental sulfur in the

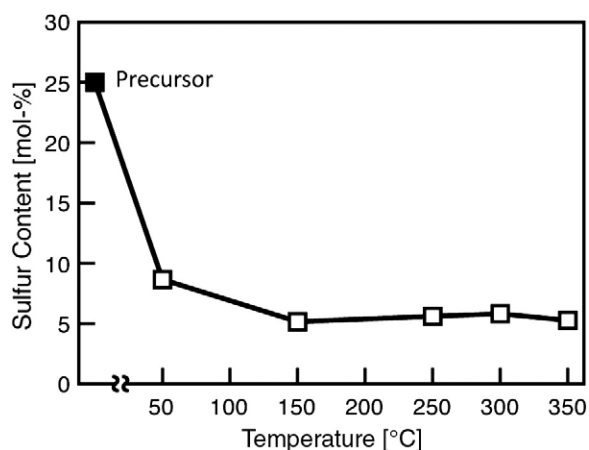


Fig. 3. Sulfur content of the precursor film measured using energy dispersive spectroscopy (EDX). The films were prepared by spin-coating from a precursor solution using 0.5 mole fraction of S, followed by thermal annealing at 50, 150, 250, 300, and 350 °C. The original sulfur contents added in the precursor solution (labeled as Precursor) are provided as a reference.

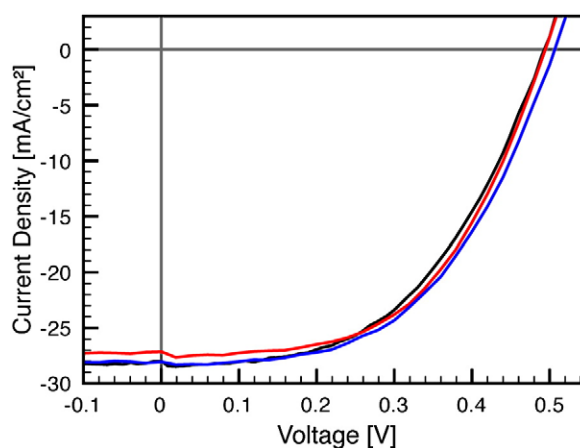


Fig. 4. J - V characteristics of the $\text{CuIn}_x\text{Se}_{2-x}$ solar cell measured under the AM 1.5 G spectrum at 100 mW/cm^2 intensity. The $\text{CuIn}_x\text{Se}_{2-x}$ layer was fabricated by four depositions of precursor solution using a 0.5 mole fraction of S with thermal annealing at 350 °C. The Cu:In ratio in the precursor solution was kept constant throughout all depositions.

Table 2

Summary of the photovoltaic properties of the three different cells.

Device	J_{SC} (mA/cm^2)	V_{OC} (mV)	FF	PCE (%)
1	28.04	500	0.53	7.41
2	27.14	500	0.54	7.30
3	28.01	500	0.50	7.05
Average	27.73	500	0.52	7.26

precursor solution as a result of reaction with hydrazine. Different reaction pathways at elevated temperature will have to be developed in order to increase the incorporation of sulfur in resulting CISS material.

The photovoltaic cell was fabricated by employing the CISS films with a S/[S + Se] of 0.13 ($E_g = 1.10$ eV). Current density-voltage (J - V) characteristics of fabricated cells under the 1-sun illuminating condition are shown in Fig. 4, and their photovoltaic properties are summarized in Table 2. The three cells were fabricated on the same substrate. The best cell yields a short-circuit current (J_{SC}), open-circuit voltage (V_{OC}), fill factor (FF), and power conversion efficiency (PCE) of 28.04 mA/cm^2 , 500 mV, 0.53, and 7.43%, respectively. The averaged values of the J_{SC} , V_{OC} , FF, and PCE over the three devices are 27.73 mA/cm^2 , 500 mV, 0.52, and 7.26%, respectively.

The observed fill factor is the major limitation for the PCE. Compared to an FF of 0.77 reported for cells deposited utilizing a three-stage process [14], this fabricated cell only achieved an averaged value of 0.51. The loss in FF is likely due to the grain size and the thickness of the absorber (CISS) layer. Both grain size and absorber thickness can be observed in the cross-sectional SEM image of the fabricated cell shown in Fig. 5. The microstructure of the absorber layer is marked by a grain size of approximately 50 nm, which is very different from that commonly observed. Small grain size provides more scattering centers for photo-generated carriers, which impedes the extraction of the carriers. The effect of grain size is also reflected in the increase in series resistance of the cell. The average series resistance of the three cells measured under dark conditions is 1.67 $\Omega\text{-cm}^2$. In addition, the thickness of the absorber layer also contributes to the loss in FF. In this work, shunting problems associated with absorber thickness are unlikely to be a problem as the films can be deposited in a smooth and dense form even at thickness <100 nm. However, there have been reports of tunneling-enhanced recombination with the thin absorber layer [15]. As the absorber layer thickness is decreased, there would be more

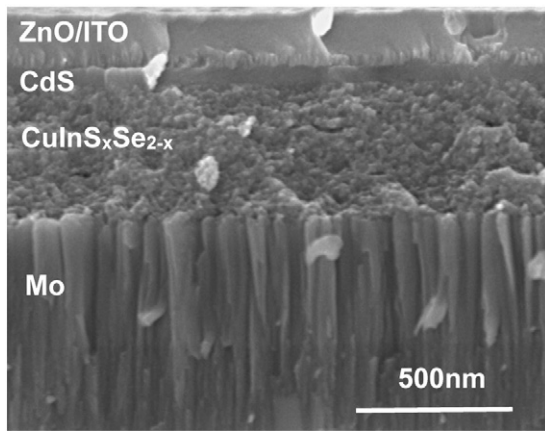


Fig. 5. Cross-sectional SEM image of the photovoltaic cell with the $\text{CuInS}_x\text{Se}_{2-x}$ layer deposited using the same parameters as described in Fig. 4.

carriers generated near the back-contact, which are subject to back-contact recombination.

4. Conclusions

The present work explored the hydrazine-based solution processing in the low-temperature regime for CISS solar cells. The presence of chalcopyrite crystallite at temperatures as low as 150 °C indicated that the hydrazine-based processing provides a different reaction pathway in forming the chalcopyrite structure from that reported using coevaporation or chalcogenization from metallic precursor layers. Sulfur incorporation to form CISS can be achieved by simply increasing the sulfur content in the precursor solution. A bandgap of 1.14 eV has been achieved; however, further increase in bandgap is limited by the difficulty of retaining sulfur in the precursor film. Photovoltaic performance of the CISS fabricated at 350 °C has demonstrated a PCE of 7.43%. This low-temperature processing provides

a viable method to fabricate cells on polyimide substrates. With further tuning of the absorber layer in order to enhance the carrier collection near the back-contact, we believe that the photovoltaic performance of cells fabricated using our methodology can be further improved.

Acknowledgments

The authors would like to acknowledge financial support from the National Science Foundation.

References

- [1] A. Rockett, R.W. Birkmire, *J. Appl. Phys.* 70 (1997) R81.
- [2] M. Powalla, B. Dimmler, *Thin Solid Films* 361–362 (2000) 540.
- [3] T. Negami, S. Nishiwaki, Y. Hashimoto, N. Kohara, Proceedings of the Second World Conference and Exhibition on Photovoltaic Solar Energy Conversion (WCPEC-2), 1998, p. 1181, Vienna, Austria.
- [4] W.N. Shafarman, R.W. Birkmire, S. Marsillac, M. Marudachalam, N. Orbey, T.W.F. Russel, Proceedings of the 26th IEEE Photovoltaic Solar Energy Conference, 1997, p. 331, Anaheim, US.
- [5] D. Rudmann, F. Haug, M. Kaelin, H. Zogg, A. Tiwari, *Mater. Res. Soc. Symp. Proc.* 668 (2001) H3.8.1.
- [6] D. Mitzi, M. Yuan, W. Liu, A. Kellock, S. Chey, L. Gignac, A.G. Schrott, *Thin Solid Films* 517 (2009) 2158.
- [7] D.J. Milliron, D.B. Mitzi, M. Copel, C.E. Murray, *Chem. Mater.* 18 (2006) 587.
- [8] W. Hou, S.H. Li, C.C. Tung, R.B. Kaner, Y. Yang, OSA Solar Energy: New Materials and Nanostructured Devices for High Efficiency, 2008, Stanford, US, SWC1.
- [9] H.A. Al-Thani, F.S. Hasoon, M. Young, S. Asher, J.L. Alleman, M.M. Al-Jassim, D.L. Williamson, Proceedings of the 26th IEEE Photovoltaic Solar Energy Conference, 2002, p. 720, New Orleans, US.
- [10] V. Shrotriya, G. Li, Y. Yao, T. Moriarty, K. Emery, Y. Yang, *Adv. Funct. Mater.* 16 (2006) 2016.
- [11] H. Neumann, *Sol. Cells* 16 (1986) 317.
- [12] M. Engelmann, B.E. McCandles, R.W. Birkmire, *Thin Solid Films* 387 (2001) 14.
- [13] D.B. Mitzi, M. Copel, S.J. Chey, *Adv. Mater.* 17 (2005) 1285.
- [14] M.A. Contreras, B. Egaas, K. Ramanathan, J. Hiltner, A. Swartzlander, F. Hasoon, R. Noufi, *Prog. Photovoltaics Res. Appl.* 7 (1999) 311.
- [15] O. Lundberg, M. Bodegard, J. Malmstrom, L. Stolt, *Prog. Photovoltaics Res. Appl.* 11 (2003) 77.